Chromatogram Analysis on Revealing Aggregated Number and Location of Gold Nanoparticles Within Living Cells

Sheng-Hann Wang · Chia-Wei Lee · Ming-Yang Pan · Shu-Yi Hsieh · Fan-Gang Tseng · Pei-Kuen Wei

Abstract We present a method to directly observe three-dimensional (3D) distribution of aggregated gold nanoparticles (Au NPs) in live cells using dark-field sectional optical microscopy with chromatographic analysis. The scattering images of clustered Au NPs were transformed from *RGB* regular coordinate to hue, saturation, and value (*HSV*) cylindrical coordinate. The hue distinguished Au NPs from scattering images of cellular organelles. The saturation eliminated the interference from the defocused spots. The value, which indicated the scattering intensity, defined the 3D locations of Au NPs. The *V/H* ratio showed a linear relation with the Au NP number in the cluster. It was applied to estimate the numbers of aggregated nanoparticles in endosome vesicles. Using the chromatographic analysis, the calculated nanoparticle numbers were in good agreement with mass spectroscopic measurement. Compared to conventional methods, the chromatographic approach provides a simple observation of 3D distribution of Au NPs and their aggregation states in living cells.

S.-H. Wang · F.-G. Tseng
Department of Engineering and System Science, National Tsing-Hua University, 101, Sec. 2, Kuang-Fu Road, Hsinchu, Taiwan

S.-H. Wang · C.-W. Lee · M.-Y. Pan · S.-Y. Hsieh · F.-G. Tseng · P.-K. Wei (✉)
Research Center for Applied Sciences, Academia Sinica, 128 Academia Road, Sec. 2, Nankang, Taipei, Taiwan
e-mail: pkwei@gate.sinica.edu.tw

M.-Y. Pan
Institute of Photonics Technologies, National Tsing-Hua University, 101, Sec. 2, Kuang-Fu Road, Hsinchu, Taiwan

P.-K. Wei
Institute of Biophotonics, National Yang-Ming University, Taipei, Taiwan

Introduction

Gold nanoparticles (Au NPs) have been widely employed in the intercellular imaging, drug/gene delivery system, and photothermal therapies over the last decades due to their good biocompatibility as well as nanoplasmonic properties [1–4]. The cellular interaction of Au NPs is typically involved with the receptor mediated endocytosis (RME). The number and distribution of those nanoparticles would change cellular responses such as the proliferation and regulation [5]. Therefore, a thorough understanding of internalized nanoparticles and their aggregated status is important for the applications. The cellular internalization of nanoparticles based on the thermodynamic and mechanic models have been made [6, 7], and some experiments have confirmed the models with different sizes and shapes of nanoparticles using inductively coupled plasma mass spectroscopy (ICP-MS) or the transmission electron microscopy (TEM) [8, 9]. Most of the studies indicated that nanoparticles with a size of 40–50 nm in diameter exhibited larger uptake efficiency than other sizes. Apart from the ICP-MS and TEM, optical microscopy, such as fluorescence and dark field microscopy, was widely used to study the interaction between Au NPs and living cells [10, 11]. However, less quantitative information of the numbers of Au NPs in the endosome vesicles was revealed by conventional optical microscopy. To overcome this quantitative problem, we developed a chromatographic analysis approach to map not only the 3D distribution of Au NPs but also their aggregated number of each cluster by a dark-field sectional optical

microscopy [12]. Au NPs provide label-free and high-contrast scattering images under dark-field illumination due to the excitation of localized surface plasmon resonance (LSPR) [13]. In addition, once two or more Au NPs are in close proximity to each other, the plasmonic coupling would occur and impart higher-order LSPR modes. The plasmonic coupling results in a red shift of peak wavelength. Using the LSPR effect and spectroscopic techniques, the cellular endocytosis of Au NPs with different aggregation states has been demonstrated. However, for the hyper-spectroscopic technique [14], it needs an additional line scan for spectroscopic image and a longer acquisition time for reading spectra from scattering signals of few Au NPs. As for the filtering imaging technique [15], it uses the intensity at different selected wavelengths to identify metal NPs. However, some large organelles have comparable intensity in the selected wavelength. In the monochromatic image, it is hard to distinguish NPs from the organelles. Both methods need additional mechanic components to map 2D images. In this work, the aggregated Au NP number is obtained by considering high-order LSPR mode instead of peak wavelength shift. A chromatogram analysis method is developed to calculate the locations together with aggregated Au NP number directly from the scatting color images. With the use of dark-field sectional optical microscopy and chromatogram analysis, the 3D distribution of Au NPs in/on living cells can be easily obtained.

The chromatogram analysis in this work is based on the color transformation from conventional red, green, and blue (RGB) regular color coordinate to hue, saturation, and value (HSV) cylindrical coordinate [16]. Different from the RGB coordinate, the HSV coordinate provides a chromatogram as a consideration of allover the optical spectrum. It is more sensitive to color changes with different aggregated numbers of Au NPs. In principle, the H represents the primary color of the spectrum, V is the overall brightness, and S is the sharpness of the spectrum. In the study of Au NPs and living cell interactions, hue value helps distinguish Au NPs from scattering images of cellular organelles. Saturation value eliminates the interference from the defocused spots. The value, which indicates the scattering intensity, helps find the 3D locations of Au NPs. It is noted that both V and H values are closely related to aggregated number of Au NPs. We found that the V/H ratio has a linear relation with the Au NP number in the cluster. It can be used to calculate the numbers of aggregated Au NPs in a living cell. In the application, we demonstrated 3D distribution and the aggregated number of each Au NPs cluster in non-small lung cancer cells with 50-nm Au NPs. This approach provides a direct observation of Au NPs of endocytosis process and a fast estimation of the aggregated status within living cells.

Methods

Materials

The 50-nm diameters of gold nanospheres were obtained from Nanopartz with original particle concentrations of approximately 4.5×10^{10} particles per milliliter, respectively. 3-Aminopropyl-triethoxysilane (APTES, $\geqq 98$ %) and poly(allylamine hydrochloride) (PAH, $M_w \sim 15,000$) were obtained from Sigma-Aldrich. All other reagents for cell culture, such as Dulbecco's modified Eagle's medium (DMEM), fetal bovine serum (FBS), and antibiotic penicillin streptomycin amphotericin (PSA), were from Invitrogen.

Functionalization of Au NPs

The commercial Au NPs were initially stabilized by citrate anions with a negative surface charged. We centrifuged those particles at 5000 rpm for 5 min to remove the excess citrate in the solution and redispersed the deposition with 200 μL of deionized water. One milliliter of 0.1 wt% poly(allyamine hydrochloride) (PAH, $M_w \sim 15,000$) was subsequently added into the citrate coated Au NPs for overnight. Then, the Au NPs were washed twice by deionized water with 5000 rpm centrifugation for 5 min each time. The UV–vis spectrum of PAH stabilized 50 nm Au NPs had a small red shift of the LSPR spectrum. In addition, the zeta potential of citrate stabilized (commercial) was −3.89±0.80, and PAH stabilized Au NPs was 13.99±1.86. Both spectra and zeta potential studies indentified the surface modification of PAH-coated Au NPs.

Optical Set-Up

The scattering images of Au NP clusters at different focal planes were taken using a dark-field sectional optical microscopy [12]. Figure 1 shows the optical set-up. A 20-W metal halide light was obliquely incident into the sample by the Cyto-Viva set-up. The 100x (N.A. 0.6-1.3) oil objective lens was mounted on a PZT micro-focusing system stage, which was controlled by a function generator to generate a zig-zag voltage ramp. When the PZT was activated, a trigger signer was simultaneously sent to the frame grabber to begin the synchronal recording of a sequence of images. The images were recorded by a high-speed color charge-coupled device (CCD) (pixelfly qe). A sequence of scattering color images at different z positions with a step size of 240 nm was recorded.

Cell Culture

Non-small cancer cells (CL1-0) were incubated on a cleaned glass slide with a density of 10^6 cells/mL for overnight. The medium was DMEM supplemented with 10 % FBS and 1 %
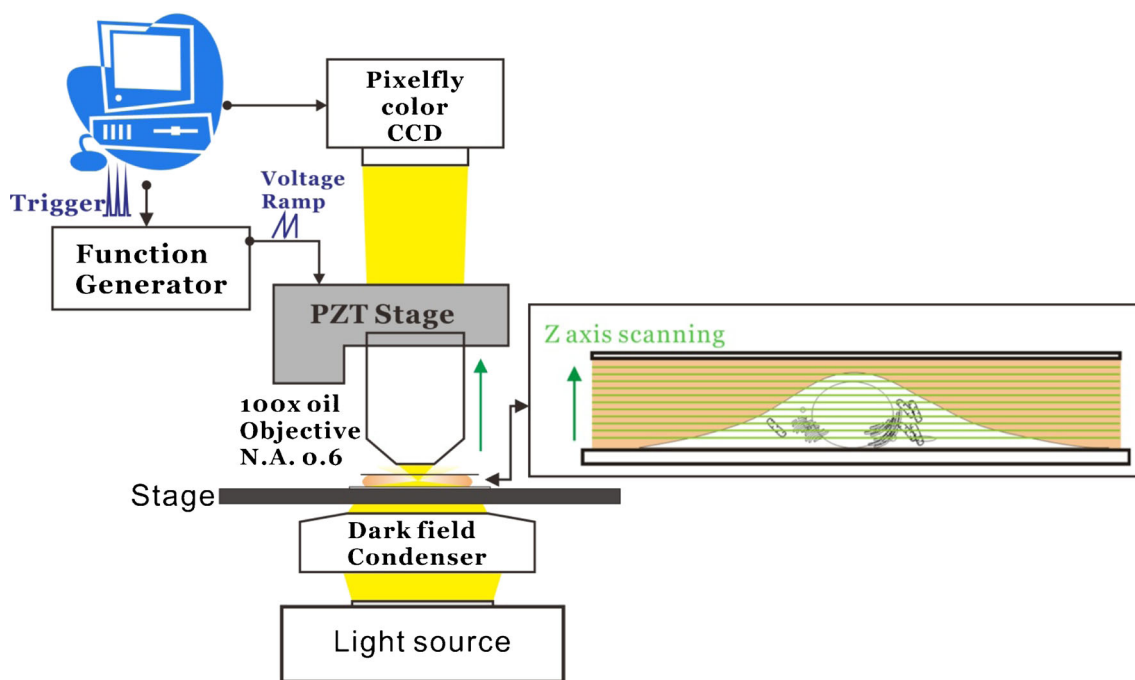
Fig. 1 The optical set-up of the dark-field sectional microscopy. All appliances were put in an incubator with a temperature of 37 °C

PSA. Cells were then treated with 0.1 nM 50-nm Au NPs coated with PAH for different incubation times.

ICP-MS Analysis

For the ICP-MS experiments, the cells were cultured in six wells culture dish at an initial density of 10^6 cells per milliliter. After 24 h, the nanoparticles were added to the medium with a final concentration of 0.2 nM. The interactions were kept for 1–5 h, respectively. Then, the cells were washed with PBS to remove the unbounded Au NPs. The trypsinized cell dispersion was sonicated for 10 min to disrupt the cell membranes. The Au NPs was dissolved by adding 0.5 mL aqua regia. The concentration of gold was determined by ICP-MS (ICP-MS Xseries II, Thermo) and converted to the number of Au NPs per cell.

Results and Discussion

Chromatogram Analysis of Clustered Au NPs

To estimate the number of Au NPs in each aggregate using chromatographic method, we first prepared submicrometer transparent holes to mimic the vesicle surroundings in cells. The submicrometer hole array was fabricated by coating 300-nm-thick polymethylmethacrylate (PMMA) polymer glass substrate. The glass substrate was pre-coated with the 3-aminopropyl-triethoxysilane (APTES) for the conjugation

with Au NPs. The electron-beam lithography was employed to make 500-nm submicrometre holes with 2-μm period on the PMMA. After the development, drops of 2 nM Au NPs were put into the submicrometer holes and placed overnight. The immobilization of Au NPs on the substrate is due to the covalent bonding of gold and amino group (the function group of APTES, while the other side of APTES bound to the glass substrate). After the immobilization process, the sample was washed with deionized water (DI water) for several times, and unbound Au NPs were removed. Au NP aggregates with different clustered numbers were formed in submicrometre holes. The colorful scattering images of clustered Au NPs surrounded with DI water were mapped using the dark-field illumination (Cyto-Viva). To compare with the color images, the scattering spectra of clustered Au NPs were also measured. The samples were dried for the investigation by a scanning electron microscope. It is noted that the arrangement of Au NPs in each hole was not changed after the drying process because of the covalent bonding of APTES. Figure 2a shows scattering images and the corresponding SEM images of Au NPs with 50 nm in diameter. Au NPs were randomly distributed in the holes. However, when there are large numbers of Au NPs in the holes, many Au NPs tend to immobilize around the aperture wall in order to occupy the largest space. The "ring" arrangement has the most possibility for large numbers of Au NPs as seen in the SEM images. Figure 2b shows corresponding spectra for different degrees of Au NPs aggregates. It shows that the peak wavelength (the LSPR band) is slightly increased from 530 to 550 nm as Au NP aggregated number increased from 1 to 18. The red shift of LSPR is a

Fig. 2 **a** List of both measured scattering images and corresponding SEM images with different assembled clusters of 50 nm Au NPs in the submicrometer holes, scale bar= 500 nm. **b** The corresponding scattering spectra (normalized) of 50 nm Au NPs shown in Fig. 3a
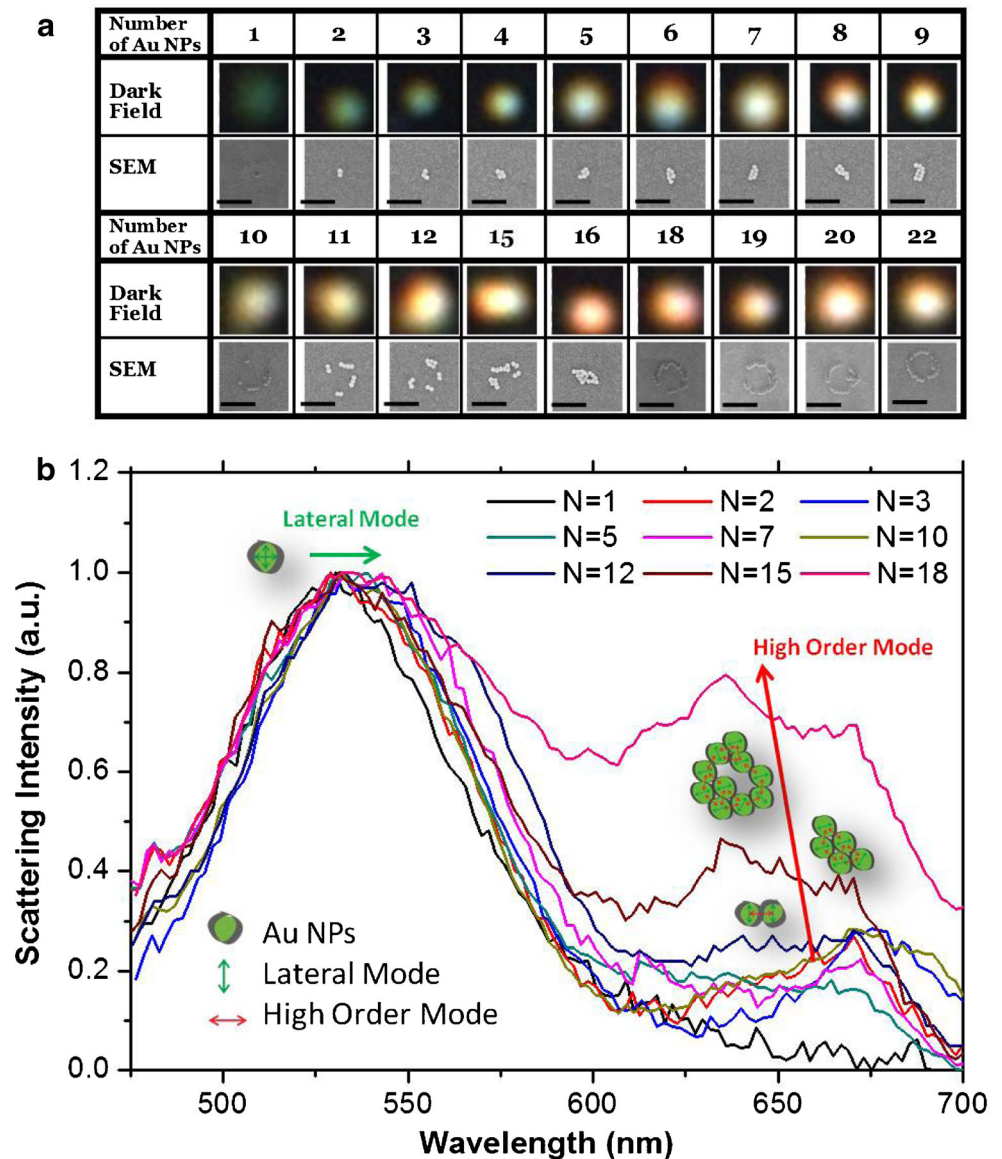
common way to determine the environmental changes of Au NPs. However, the color change from the LSPR red shift is too small to be detected by the color CCD. As indicated in Fig. 2b, there are two resonant peaks of aggregated Au NPs in the visible range. The dominant LSPR (peaked at ~550 nm) is the fundamental mode (lateral mode). The second speak is the high-order mode due to the strong plasmonic coupling of neighboring Au NPs (peaked at 600–700 nm) [17]. The intensity of high-order mode increases with the aggregated Au NP number. For the color CCD, the dominant LSPR mode is recorded by green pixel and the high-order mode is read by red pixel. As the number of Au NPs in the submicrometer holes increases, the scattering color changes from green, yellow to orange. Such color change can be acted as the agent to distinguish the aggregate states.

In order to obtain the relation between the color and aggregated number of Au NPs, we measured both *hue* and *value*,

which indicated the color and brightness, respectively. Figure 3 shows the results. The *H* value is considered as the weighted mean of the wavelength, and it is sensitive to color changes with different Au NP aggregates. The *V* value is related to the scattering cross-section of Au NPs, i.e., the brightness and which is also sensitive to aggregated Au NP numbers. Figure 3a shows the statistical results of *H* and *V* values as a function of Au NP numbers. Owing to the increase of high-order modes, the color with increasing aggregated number shows decreased *H* value. On the other hand, *V* is increased due to the increase of Au NP numbers. Both *H* and *V* curves are not linear to the Au NP numbers. The values become saturated for large Au NP numbers. It is noted that error would be large if only the intensity or hue curve is used as the reference for estimating Au NP numbers. Since both *H* and *V* values have opposite changes with the increase in Au NP numbers, we thus use the ratio of brightness to hue (*V*/*H*)
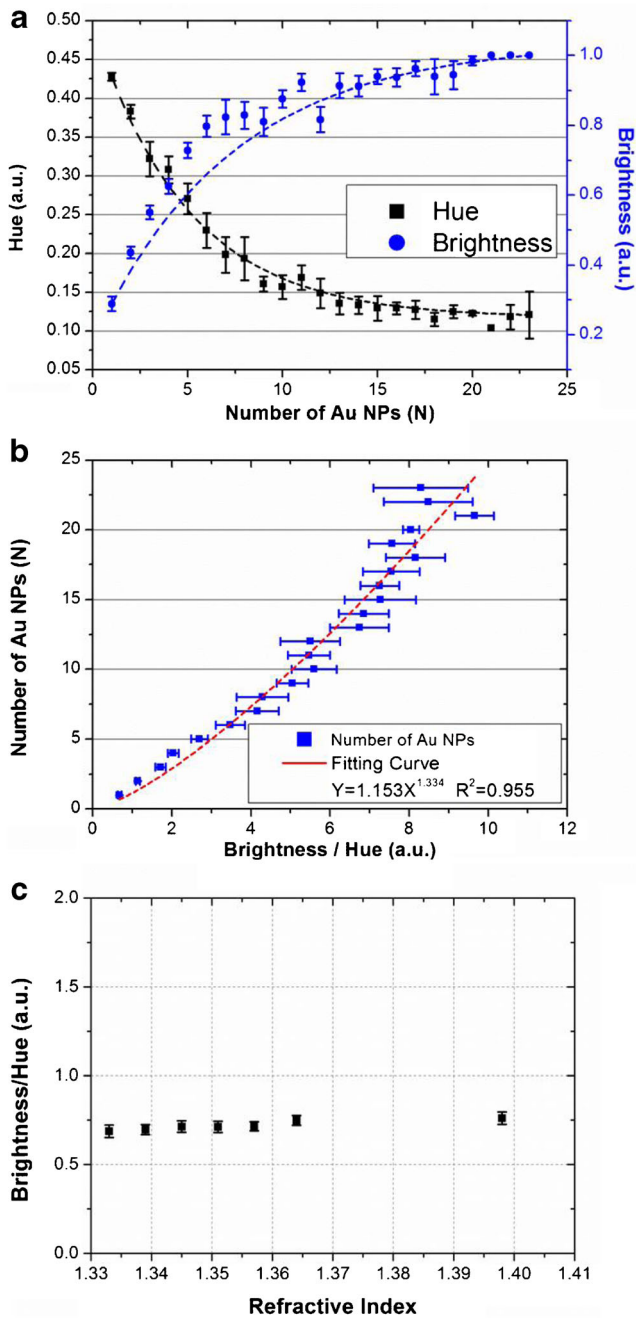
Fig. 3 **a** The hue and brightness and **b** the ratio of brightness to hue for different clustered 50-nm Au NPs. **c** The ratio of brightness to hue with different surrounding refractive index for individual Au NPs. Data are presented as mean±standard deviation. $n \geqq 30$ for each sample

as an indicator for the aggregated number. Figure 3b shows the V/H as a function of 50-nm Au NP numbers. The ratio shows a linear response with the aggregated NPs. The ratio has a better sensitivity to the Au NP numbers than the consideration of only H or V value.

In the experiment, we put different Au NP aggregates in submicrometer holes. The samples were covered with water. The surroundings of Au NPs were the water and the substrate. The LSPR of Au NPs is changed with the environmental

refractive index. However, the typical wavelength shift of LSPR in different surrounding medium is only few nanometers. The change in the hue value is very small. Figure 3c shows the brightness/hue values surrounded with different environment refractive index (adjusted by preparing different percentage of glycerol in DI water) of individual Au NPs. The surrounding refractive index only has a slight effect on the brightness/hue value. On the other hand, the LSPR is also sensitive to the NP arrangement. When Au NPs are close to each other, high-order LSPR mode occurs. It results in a substantial increase in scattering intensity in the red light region. The change in the hue value is large as seen in Fig. 3a. Therefore, we employed this hue value together with the scattering brightness to statistically obtain the Au NP numbers in the aggregate. It is noted that the surrounding medium of Au NPs would be different in cells and in the PMMA holes. However, the proposed chromatographic method is only sensitive to aggregated number of Au NPs and not sensitive to the environmental refractive index. Therefore, the chromatogram analysis method can be applied to different surrounding medium of Au NPs.

Three-Dimensional Distribution of Au NP Aggregates in Living Cells

For the distributions of Au NPs in 3D space with living cells, the brightness was used to define the location, and the V/H was used to indicate the Au NP aggregated numbers. Compared to RGB color space, HSV images provide advantages to distinguish cellular organelles and defocused spots from Au NPs. Large organelles have scattering intensities equal or larger than the scattering intensities of Au NPs. Nevertheless, their *hue* is much higher than the colorful Au NPs. Using the *hue* can help distinguish Au NPs from complex organelle environment. Figure 4a shows the original *RGB* image of Au NPs within a living cell. It shows different colorful bright scattering spots. The scattering of organelles presents as blue and white due to the Raleigh and Mie scattering. The Au NPs show green, yellow, and orange colors due to the LSPR and plasmonic coupling effects. We transformed the image into the *HSV* space via a Matlab program code "rgb2hsv." Figure 4b shows Au NPs exhibit a much lower *hue* than organelles. Therefore, we can exclude bright spots of cellular organelles using a smaller H values. For the 3D mapping of Au NPs, the defocused Au NPs would form some halos. Both the halos would also influence the calculation of Au NP numbers. To exclude the non-Au NPs and sharpen the images, both hue and saturation are used as filters [18]. By setting a suitable threshold, the organelles and halos spots can be eliminated as shown in Fig. 4c. Using the V/H, the aggregated number of Au NPs in this focused plane can be calculated as shown in Fig. 4d.

The 3D locations of Au NP spots can be determined according to their intensity distribution as discussed in our
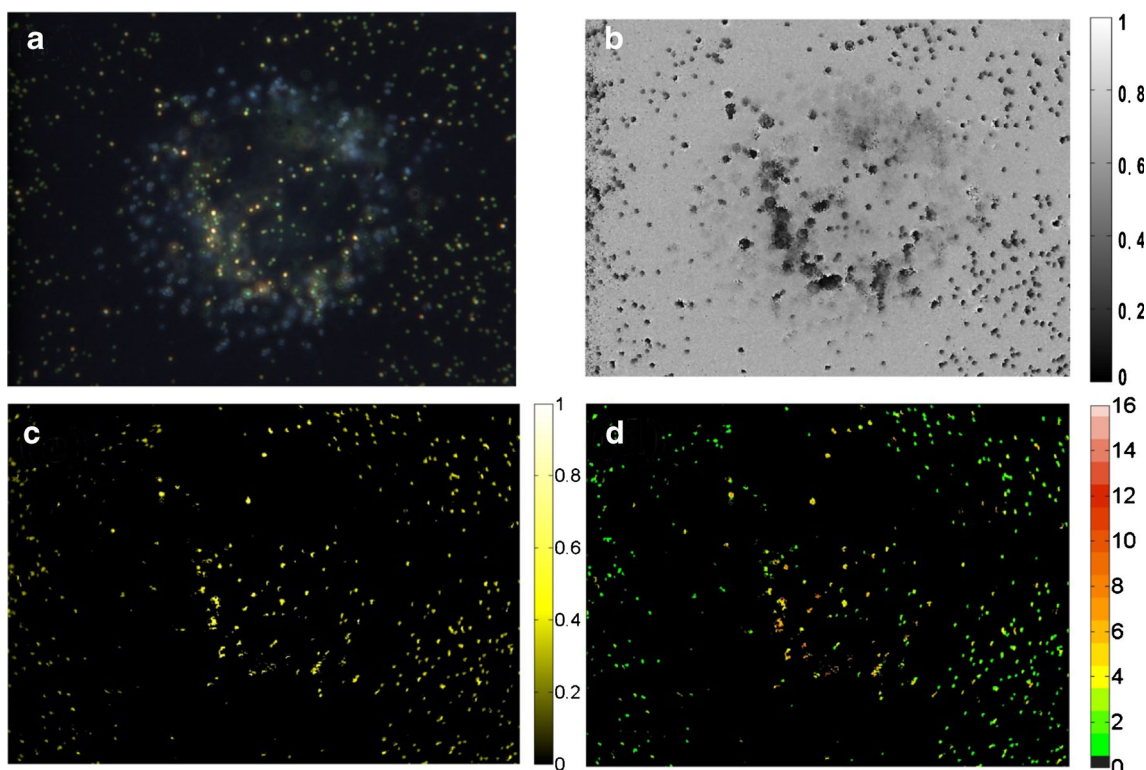
Fig. 4 The images of Au NPs in a living cell using regular *RGB* and cylindrical *HSV* method. **a** An original *RGB* scattered image of cell treated with Au NPs (50 nm) under the dark-field illumination. The *RGB* image was then converted to *HSV* image. **b** The *hue image.* The Au NP presents a lower *hue* value than organelles. **c** The brightness image. The organelles and halos were filtered out by setting thresholds for both *hue* and *saturation* values. **d** The *V/H* for the each spots of Au NPs

previous report [12]. Briefly, a stack of image sequence with different focused plane was first recorded as shown in Fig. 5a. The *X–Y* positions of the spots were determined by projecting all the images onto the same plane. The *Z* positions of the spots were obtained by fitting the intensity curve with a Gaussian profile of the stack of images to find the maximum position. Then, the 3D positions of those Au NPs aggregates were consequently determined. By further applying the cross-

Fig. 5 **a** A sequence of optical scattering images at different *z* positions with a step size of 240 nm. The color images were obtained by the dark-field sectional optical microscopy. **b** The 3D reconstruction of the distribution of Au NP spots from a sequence of optical scattering images. The *color bar* indicates the Au NP numbers in the spot. **c** Cross-sectional view of **b**. **d** The illustration of the endocytic trafficking of nanoparticles
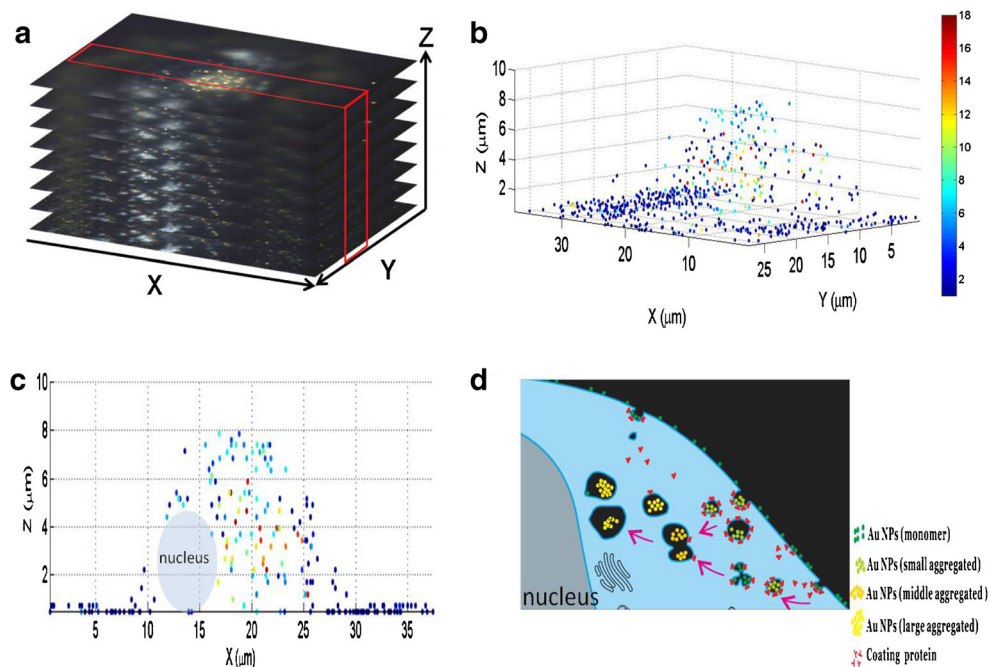
reference of the *V/H* for each spot, the Au NP distribution together with their aggregated status was mapped as shown in Fig. 5b. The corresponding Au NP number in each spot is shown in the color bar. Figure 5c shows cross-sectional images of the Au NPs and their aggregated states. Most single Au NPs distributed on the glass surface. It can be found that aggregates with few Au NPs were near the cell membrane, while large aggregated numbers of Au NPs were near the cell nucleus. Figure 5d illustrates the process of endocytosis of Au NPs. Along the endocytic pathway of nanoparticles, the early endosomal network is a vesicle fusion cascade, in which the dominant effect is the continuous merger of small vesicles into larger ones, which carry more and more Au NPs cargos in the vesicle. The increase in aggregated Au NPs inside the cells is due to the fusion of endocytic vesicles. The result is consistent with the receptor-mediated endocytosis for nanoparticles [19].

Comparison of Total Number of Au NPs with ICP-MS

The chromatic analysis method can be applied to estimate the total number of Au NPs in cells. We compared the numbers of Au NPs with the results obtained by ICP-MS method. For the ICP-MS experiments, the cells were cultured in dishes with the same cell density, 10^6 cells/mL. The cultured time and treated concentration of Au NPs were the same as the experiments in chromatic analysis method. The cells were then washed with PBS to remove the unbounded Au NPs. The trypsinized cell dispersion was subsequently sonicated for 10 min to disrupt the cell membranes. The Au NPs were dissolved by adding 0.5 mL aqua regia. The concentration of gold was determined by ICP-MS (ICP-MS Xseries II, Thermo) and converted to the number of Au NPs per cell.

We quantified the 50-nm Au NP numbers for different culture times, 1–5 h. Figure 6 shows the statistical result. As the interaction time increases, more Au NPs are found in the cells. Both data show similar statistical results. The quantitative numbers are consistent with previous studies as presented by Chithrani and Cho [8, 20]. It is noted that the ICP-MS method included many Au NPs deposited on the substrate. For the chromatogram analysis method, only the Au NPs on/in cells are calculated. Therefore, the total numbers of Au NPs and the error bars for IC-MS are larger than those for the proposed chromatic method.

Conclusions

In summary, we discussed the relationship between scattering colors and aggregated numbers of Au NPs. Owing to the increase in the high-order mode in the red light range with increasing number of aggregated Au NPs, the scattering color presents a significant chromatic changes. Using a chromatographic analysis based on the color image transformation (*RGB* to *HSV*), aggregated Au NPs in living cells can be located and counted. Through the calibration of known numbers of Au NPs by SEM and dark-field microscopy, we established the chromatogram as a function of aggregated Au NP numbers. The *V/H* ratio showed a linear relation with the Au NP number in the cluster. We demonstrated the application for studying the endocytic trafficking of nanoparticles. The large aggregated nanoparticles near the nucleus verified the fusion the endocytic vesicles. Using the chromatographic analysis, the calculated nanoparticle numbers were in good

Fig. 6 The statistics of total Au NP number per cell measured by chromatogram method and ICP-MS method. The Au NPs were 50 nm in diameter and interacted with CL1-0 cells. For the chromatogram analysis, cell number >30
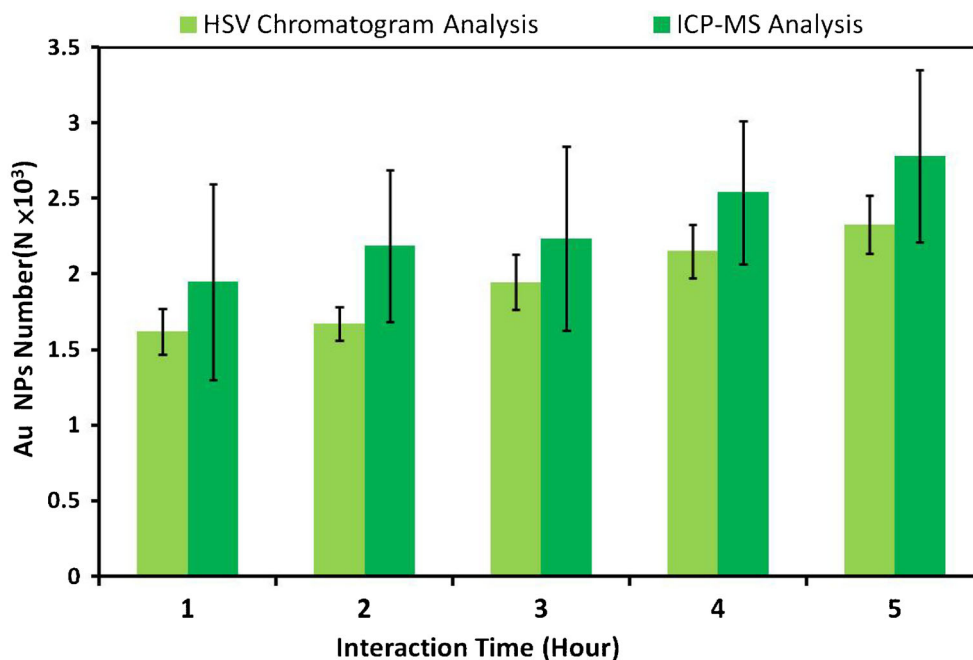
agreement with mass spectroscopic measurement. Compared with other approaches, the chromatographic approach provides an easy and fast measurement of 3D distribution of aggregated Au NP numbers within living cells. This method could further reinforce the capacity in quantitative analysis of a long-term living cell–Au NPs interaction using an optical system.

References

1. Hutter E, Maysinger D (2011) Gold nanoparticles and quantum dots for bioimaging. Microsc Res Tech 74:592–604
2. Cheng J, Gu YJ, Cheng SH, Wong WT (2013) Surface functionalized gold nanoparticles for drug delivery. J Biomed Nanotechnol 9:1362–1369
3. Xu L, Liu Y, Chen Z, Li W, Liu Y, Wang L, Liu Y, Wu X, Ji Y, Zhao Y, Ma L, Shao Y, Chen C (2012) Surface-engineered gold nanorods: promising DNA vaccine adjuvant for HIV-1 treatment. Nano Lett 12:2003–2012
4. El-Sayed IH, Huang X, El-Sayed MA (2006) Selective laser photothermal therapy of epithelial carcinoma using anti-EGFR antibody conjugated gold nanoparticles. Cancer Lett 239:129–135
5. Unfried K, Albrecht C, Klotz L-O, Mikecz AV, Grether-Beck S, Schins RPF (2007) Cellular responses to nanoparticles: target structures and mechanisms. Nanotoxicology 1:52–71
6. Gao HJ, Shi WD, Freund LB (2005) Mechanics of receptor-mediated endocytosis. PNAS 102:9469–9474
7. Decuzzi P, Ferrari M (2007) The role of specific and non-specific interactions in receptor-mediated endocytosis of nanoparticles. Biomaterials 28:2915–2922
8. Chithrani BD, Ghazani AA, Chan WCW (2006) Determining the size and shape dependence of gold nanoparticle uptake into mammalian cells. Nano Lett 6:662–668
9. Chithrani BD, Chan WCW (2007) Elucidating the mechanism of cellular uptake and removal of protein-coated gold nanoparticles of different sizes and shapes. Nano Lett 7:1542–1550
10. Qian W, Huang X, Kang B, El-Sayed MA (2010) Dark-field light scattering imaging of living cancer cell component from birth through division using bioconjugated gold nanoprobes. J Biomed Opt 15:046025–046025
11. Jiang W, Kim BYS, Rutka JT, Chan WCW (2008) Nanoparticle-mediated cellular response is size-dependent. Nat Nanotechnol 3:145–150
12. Lee CW, Chen MJ, Cheng JY, Wei PK (2009) Morphological studies of living cells using gold nanoparticles and dark-field optical section microscopy. J Biomed Opt 14:034016
13. van Dijk MA, Tchebotareva AL, Orrit M, Lippitz M, Berciaud S, Lasne D, Cognet L, Lounis B (2006) Absorption and scattering microscopy of single metal nanoparticles. Phys Chem Chem Phys 8:3486–3495
14. Aaron J, Travis K, Harrison N, Sokolov K (2009) Dynamic imaging of molecular assemblies in live cells based on nanoparticle plasmon resonance coupling. Nano Lett 9:3612–3618
15. Wang H, Rong G, Yan B, Yang L, Reinhard BM (2011) Optical sizing of immunolabel clusters through multispectral plasmon coupling microscopy. Nano Lett 11:498–504
16. Du C-J, Sun D-W (2005) Comparison of three methods for classification of pizza topping using different colour space transformations. J Food Eng 68:277–287
17. Herrmann LO, Valev VK, Aizpurua J, Baumberg JJ (2013) Self-sifting of chain plasmons: the complex optics of Au nanoparticle clusters. Opt Express 21:32377–32385
18. Strickland RN, Kim C-S, McDonnell WF (1987) Digital color image enhancement based on the saturation component. Opt Eng 26:609–616
19. Brandenberger C, Mühlfeld C, Ali Z, Lenz A-G, Schmid O, Parak WJ, Gehr P, Rothen-Rutishauser B (2010) Quantitative evaluation of cellular uptake and trafficking of plain and polyethylene glycol-coated gold nanoparticles. Small 6:1669–1678
20. Cho EC, Xie JW, Wurm PA, Xia YN (2009) Understanding the role of surface charges in cellular adsorption versus internalization by selectively removing gold nanoparticles on the cell surface with a I$_2$/KI etchant. Nano Lett 9:1080–1084